Search for pair-production of long-lived heavy charged particles in e⁺e⁻ annihilation

The ALEPH Collaboration

Abstract

A search for pair-production of long-lived, heavy, singly-charged particles has been performed with data collected by the ALEPH detector at a centre-of-mass energy of 172 GeV. Data at $\sqrt{s} = 161$, 136, and 130 GeV are also included to improve the sensitivity to lower masses. No candidate is found in the data. A model-independent 95% confidence level upper limit on the production cross section at 172 GeV of 0.2–0.4 pb is derived for masses between 45 and 86 GeV/c^2. This cross section limit implies, assuming the MSSM, a lower limit of 67 (69) GeV/c^2 on the mass of right- (left-) handed long-lived scalar taus or scalar muons and of 86 GeV/c^2 on the mass of long-lived charginos.

(submitted to Physics Letters B)

---

*See the following pages for the list of authors.

The ALEPH Collaboration

R. Barate, D. Buskulic, D. Decamp, P. Ghez, C. Goy, J.-P. Lees, A. Lucotte, M.-N. Minard, J.-Y. Nief, B. Pietrzyk

Laboratoire de Physique des Particules (LAPP), IN^{2}P^3-CNRS, 74019 Annecy-le-Vieux Cedex, France

M.P. Casado, M. Chmeissani, P. Comas, J.M. Crespo, M. Delfino, E. Fernandez, M. Fernandez-Bosman, Ll. Garrido,[15] A. Juste, M. Martinez, R. Miquel, Ll.M. Mir, S. Orteu, C. Padilla, I.C. Park, A. Pascual, J.A. Perlas, I. Riu, F. Sanchez, F. Teubert

Institut de Física d'Altes Energies, Universitat Autònoma de Barcelona, 08193 Bellaterra (Barcelona), Spain[7]

A. Colaleo, D. Creanza, M. de Palma, G. Gelao, G. Iaselli, G. Maggi, M. Maggi, N. Marinelli, S. Nuzzo, A. Ranieri, G. Raso, F. Ruggieri, G. Selvaggi, L. Silvestris, P. Tempesta, A. Tricomi,[3] G. Zito

Dipartimento di Fisica, INFN Sezione di Bari, 70126 Bari, Italy

X. Huang, J. Lin, Q. Ouyang, T. Wang, Y. Xie, R. Xu, S. Xue, J. Zhang, L. Zhang, W. Zhao

Institute of High-Energy Physics, Academia Sinica, Beijing, The People's Republic of China[8]

D. Abbaneo, R. Alemany, A.O. Bazarko,[1] U. Becker, P. Bright-Thomas, M. Cattaneo, F. Cerutti, G. Dissertori, H. Drevermann, R.W. Forty, M. Frank, R. Hagelberg, J.B. Hansen, J. Harvey, P. Janot, B. Jost, E. Kneringer, J. Knobloch, I. Lehraus, G. Lutters, P. Mato, A. Minten, L. Moneta, A. Pacheco, J.-F. Pusztaszeri,[21] F. Ranjard, G. Rizzo, L. Rolandi, D. Schlatter, M. Schmitt, O. Schneider, W. Tejessy, I.R. Tomalin, H. Wachsmuth, A. Wagner

European Laboratory for Particle Physics (CERN), 1211 Geneva 23, Switzerland

Z. Ajaltouni, A. Barrès, C. Boyer, A. Falvard, C. Ferdi, P. Gay, C . Guicheney, P. Henrard, J. Jousset, B. Michel, S. Monteil, J-C. Montret, D. Pallin, P. Perret, F. Podlyski, J. Proriol, P. Rosnet, J.-M. Rossignol

Laboratoire de Physique Corpusculaire, Université Blaise Pascal, IN^{2}P^3-CNRS, Clermont-Ferrand, 63177 Aubière, France

T. Fearnley, J.D. Hansen, J.R. Hansen, P.H. Hansen, B.S. Nilsson, B. Rensch, A. Wäänänen

Niels Bohr Institute, 2100 Copenhagen, Denmark[9]

G. Daskalakis, A. Kyriakis, C. Markou, E. Simopoulou, A. Vayaki

Nuclear Research Center Demokritos (NRCD), Athens, Greece

A. Blondel, J.C. Brient, F. Machefert, A. Rougé, M. Rumpf, A. Valassi,[6] H. Videau

Laboratoire de Physique Nucléaire et des Hautes Energies, Ecole Polytechnique, IN^{2}P^3-CNRS, 91128 Palaiseau Cedex, France

E. Focardi, G. Parrini, K. Zachariadou

Dipartimento di Fisica, Università di Firenze, INFN Sezione di Firenze, 50125 Firenze, Italy

R. Cavanaugh, M. Corden, C. Georgiopoulos, T. Huehn, D.E. Jaffe

Supercomputer Computations Research Institute, Florida State University, Tallahassee, FL 32306-4052, USA [13,14]

A. Antonelli, G. Bencivenni, G. Bologna,[4] F. Bossi, P. Campana, G. Capon, D. Casper, V. Chiarella, G. Felici, P. Laurelli, G. Mannocchi,[5] F. Murtas, G.P. Murtas, L. Passalacqua, M. Pepe-Altarelli

Laboratori Nazionali dell'INFN (LNF-INFN), 00044 Frascati, Italy

L. Curtis, S.J. Dorris, A.W. Halley, I.G. Knowles, J.G. Lynch, V. O'Shea, C. Raine, J.M. Scarr, K. Smith, P. Teixeira-Dias, A.S. Thompson, E. Thomson, F. Thomson, R.M. Turnbull

Department of Physics and Astronomy, University of Glasgow, Glasgow G12 8QQ,United Kingdom[10]

C. Geweniger, G. Graefe, P. Hanke, G. Hansper, V. Hepp, E.E. Kluge, A. Putzer, M. Schmidt, J. Sommer, K. Tittel, S. Werner, M. Wunsch

Institut für Hochenergiephysik, Universität Heidelberg, 69120 Heidelberg, Fed. Rep. of Germany[16]

R. Beuselinck, D.M. Binnie, W. Cameron, P.J. Dornan, M. Girone, S. Goodsir, E.B. Martin, P. Morawitz, A. Moutoussi, J. Nash, J.K. Sedgbeer, A.M. Stacey, M.D. Williams

Department of Physics, Imperial College, London SW7 2BZ, United Kingdom[10]

P. Girtler, D. Kuhn, G. Rudolph

Institut für Experimentalphysik, Universität Innsbruck, 6020 Innsbruck, Austria[18]

A.P. Betteridge, C.K. Bowdery, P. Colrain, G. Crawford, A.J. Finch, F. Foster, G. Hughes, R.W. Jones, T. Sloan, E.P. Whelan, M.I. Williams

Department of Physics, University of Lancaster, Lancaster LA1 4YB, United Kingdom[10]

C. Hoffmann, K. Jakobs, K. Kleinknecht, G. Quast, B. Renk, E. Rohne, H.-G. Sander, P. van Gemmeren, C. Zeitnitz

Institut für Physik, Universität Mainz, 55099 Mainz, Fed. Rep. of Germany[16]

J.J. Aubert, C. Benchouk, A. Bonissent, G. Bujosa, D. Calvet, J. Carr, P. Coyle, C. Diaconu, N. Konstantinidis, O. Leroy, F. Motsch, P. Payre, D. Rousseau, M. Talby, A. Sadouki, M. Thulasidas, A. Tilquin, K. Trabelsi

Centre de Physique des Particules, Faculté des Sciences de Luminy, IN^2P^3-CNRS, 13288 Marseille, France

M. Aleppo, F. Ragusa[12]

Dipartimento di Fisica, Università di Milano e INFN Sezione di Milano, 20133 Milano, Italy.

R. Berlich, W. Blum, V. Büscher, H. Dietl, G. Ganis, C. Gotzhein, H. Kroha, G. Lütjens, G. Lutz, W. Männer, H.-G. Moser, R. Richter, A. Rosado-Schlosser, S. Schael, R. Settles, H. Seywerd, R. St. Denis, H. Stenzel, W. Wiedenmann, G. Wolf

Max-Planck-Institut für Physik, Werner-Heisenberg-Institut, 80805 München, Fed. Rep. of Germany[16]

J. Boucrot, O. Callot,[12] S. Chen, A. Cordier, M. Davier, L. Duflot, J.-F. Grivaz, Ph. Heusse, A. Höcker, A. Jacholkowska, M. Jacquet, D.W. Kim,[2] F. Le Diberder, J. Lefrançois, A.-M. Lutz, I. Nikolic, M.-H. Schune, S. Simion, E. Tournefier, J.-J. Veillet, I. Videau, D. Zerwas

Laboratoire de l'Accélérateur Linéaire, Université de Paris-Sud, IN^2P^3-CNRS, 91405 Orsay Cedex, France

P. Azzurri, G. Bagliesi, G. Batignani, S. Bettarini, C. Bozzi, G. Calderini, M. Carpinelli, M.A. Ciocci, V. Ciulli, R. Dell'Orso, R. Fantechi, I. Ferrante, A. Giassi, A. Gregorio, F. Ligabue, A. Lusiani, P.S. Marrocchesi, A. Messineo, F. Palla, G. Sanguinetti, A. Sciabà, P. Spagnolo, J. Steinberger, R. Tenchini, G. Tonelli,[20] C. Vannini, A. Venturi, P.G. Verdini

Dipartimento di Fisica dell'Università, INFN Sezione di Pisa, e Scuola Normale Superiore, 56010 Pisa, Italy

G.A. Blair, L.M. Bryant, J.T. Chambers, Y. Gao, M.G. Green, T. Medcalf, P. Perrodo, J.A. Strong, J.H. von Wimmersperg-Toeller

Department of Physics, Royal Holloway & Bedford New College, University of London, Surrey TW20 OEX, United Kingdom[10]

D.R. Botterill, R.W. Clifft, T.R. Edgecock, S. Haywood, P. Maley, P.R. Norton, J.C. Thompson, A.E. Wright

Particle Physics Dept., Rutherford Appleton Laboratory, Chilton, Didcot, Oxon OX11 OQX, United Kingdom[10]

B. Bloch-Devaux, P. Colas, B. Fabbro, W. Kozanecki, E. Lançon, M.C. Lemaire, E. Locci, P. Perez, J. Rander, J.-F. Renardy, A. Rosowsky, A. Roussarie, J.-P. Schuller, J. Schwindling, A. Trabelsi, B. Vallage

CEA, DAPNIA/Service de Physique des Particules, CE-Saclay, 91191 Gif-sur-Yvette Cedex, France[17]

S.N. Black, J.H. Dann, H.Y. Kim, A.M. Litke, M.A. McNeil, G. Taylor

Institute for Particle Physics, University of California at Santa Cruz, Santa Cruz, CA 95064, USA[19]

C.N. Booth, R. Boswell, C.A.J. Brew, S. Cartwright, F. Combley, M.S. Kelly, M. Lehto, W.M. Newton, J. Reeve, L.F. Thompson

Department of Physics, University of Sheffield, Sheffield S3 7RH, United Kingdom[10]

K. Affholderbach, A. Böhrer, S. Brandt, G. Cowan, J. Foss, C. Grupen, P. Saraiva, L. Smolik, F. Stephan

Fachbereich Physik, Universität Siegen, 57068 Siegen, Fed. Rep. of Germany[16]

M. Apollonio, L. Bosisio, R. Della Marina, G. Giannini, B. Gobbo, G. Musolino

Dipartimento di Fisica, Università di Trieste e INFN Sezione di Trieste, 34127 Trieste, Italy

J. Putz, J. Rothberg, S. Wasserbaech, R.W. Williams

Experimental Elementary Particle Physics, University of Washington, WA 98195 Seattle, U.S.A.

S.R. Armstrong, E. Charles, P. Elmer, D.P.S. Ferguson, S. González, T.C. Greening, O.J. Hayes, H. Hu, S. Jin, P.A. McNamara III, J.M. Nachtman, J. Nielsen, W. Orejudos, Y.B. Pan, Y. Saadi, I.J. Scott, J. Walsh, Sau Lan Wu, X. Wu, J.M. Yamartino, G. Zobernig

Department of Physics, University of Wisconsin, Madison, WI 53706, USA[11]

1 Introduction

Most searches for supersymmetric (SUSY) [1] particles assume that the lightest supersymmetric particle (LSP) is neutral and weakly interacting [2] and that all charged SUSY particles ultimately decay, with a very small lifetime, into the LSP plus "standard" particles. In the hypothesis of R-parity conservation, this suggests missing energy as a possible signature of SUSY.

Nevertheless, the possibility of supersymmetric long-lived charged particles which are not strongly interacting is favoured by some interesting classes of models. In Ref. [3], for example, a scenario is proposed in which the slepton is the next-to-lightest supersymmetric particle (NLSP). The slepton can decay into a standard lepton plus a Goldstino ($\tilde{\ell} \to \ell \tilde{G}$) with a lifetime dependent on the SUSY-breaking energy scale $\sqrt{F}$:

$$c\tau \simeq (130 \ \mu\mathrm{m}) \left(\frac{100 \ \mathrm{GeV}/c^2}{m_{\tilde{\ell}}} \right)^5 \left(\frac{\sqrt{F}}{100 \ \mathrm{TeV}} \right)^4 .$$

Hence at LEP 2 centre-of-mass energies, if $\sqrt{F}$ is larger than a few thousand TeV, a 70 GeV/c^2 slepton has a decay length greater than 10 meters, which corresponds to the typical size of the detectors of the LEP experiments.

Even in the minimal supersymmetric model (MSSM) a mass degeneracy of a few hundred MeV/c^2 or less between the lightest chargino and the lightest neutralino could also induce a chargino lifetime long enough for the particle to decay outside the detector. This degeneracy may arise in some regions of the MSSM parameter space when relaxing the gauge unification condition ($M' = \frac{5}{3} M \tan^2 \theta_W$ where M' and M are the bino and wino masses).

In R-parity violating SUSY models the possibility of long-lived charged weakly interacting particles also exists. If, for example, the slepton is the LSP a single dominant baryon-number violating coupling via the operator $\bar{U}\bar{D}\bar{D}$ [4] would give a long lifetime to the slepton.

At LEP 1, searches for heavy stable charged particles were performed by DELPHI [5], OPAL [6] and ALEPH [7], which sets the most stringent LEP 1 upper limit on the production cross section, roughly 1.5 pb at 95% CL for masses between 34 and 44 GeV/c^2. DELPHI [8] has analysed data collected at energies up to $\sqrt{s} = 172$ GeV, setting a limit of ~ 0.3–0.5 pb for masses between 45 and 85 GeV/c^2.

This letter presents the results of a search for pair-production of long-lived, singly-charged, not strongly interacting particles with mass greater than 45 GeV/c^2. The analysis is performed using data collected during the second 1996 LEP running period, at $\sqrt{s} = 172$ GeV. To increase the sensitivity for low masses, data collected at 161 GeV (the first 1996 running period) and 130, 136 GeV (the 1995 high-energy run) are also analysed.

The selection is based on kinematic criteria related to the pair-production hypothesis, and on the specific energy-loss measurement (dE/dx), a powerful tool for exploring the high-mass region. When the mass of the heavy particles approaches the kinematic limit, the energy loss becomes high enough to saturate the main tracking detector's electronics. To recover this interesting mass region, a selection based on the search for saturated signals in the tracking detector has been developed.

Limits on the cross section are translated into lower limits on the masses of long-lived slepton and charginos based on the production cross sections predicted by the MSSM.

2   The ALEPH detector

A detailed description of the ALEPH detector can be found in Ref. [9], and an account of its performance as well as a description of the standard analysis algorithms in Ref. [10]. Only a brief overview is given here.

Charged particles are detected in the central part of the detector consisting of a silicon vertex detector, a drift chamber (ITC) and a time projection chamber (TPC), all immersed in a 1.5 T axial magnetic field provided by a superconducting solenoidal coil. A $1/p_{\mathrm{T}}$ resolution of $6 \times 10^{-4} (\mathrm{GeV}/c)^{-1}$ is measured.

The TPC sense wires provide up to 338 measurements of the specific ionization, dE/dx, for each track. To ensure a reliable dE/dx measurement, tracks in this analysis are required to have at least 50 associated wire hits.

Between the TPC and the coil, an electromagnetic calorimeter (ECAL) is used to identify electrons and photons and to measure their energy, complemented by luminosity calorimeters (LCAL and SICAL) in the small polar angle region. The iron return yoke is instrumented to provide a measurement of the hadronic energy (HCAL) and, together with external chambers, muon identification.

The two main ALEPH triggers relevant for this analysis are based on the coincidence between a track candidate in the ITC and an energy deposit in the ECAL or HCAL modules to which the track is pointing.

3   Data and Monte Carlo samples

Data collected at $\sqrt{s} = 172^{1}$, 161, 136, and 130 GeV are analysed, corresponding to integrated luminosities of 10.6, 11.1, 2.9, and 2.9 pb^{-1}, respectively.

All major background reactions are generated at 161 and 172 GeV using the full detector simulation. These include the annihilation processes $\mathrm{e^{+}e^{-}} \rightarrow \mathrm{f\bar{f}}(\gamma)$ and the various processes leading to four-fermion final states ($\mathrm{e^{+}e^{-}} \rightarrow \mathrm{W^{+}W^{-}}$, $\mathrm{e^{+}e^{-}} \rightarrow \mathrm{We}\nu$, $\mathrm{e^{+}e^{-}} \rightarrow \mathrm{Ze^{+}e^{-}}$ and $\mathrm{e^{+}e^{-}} \rightarrow \mathrm{Z}\gamma^{*}$). These samples correspond to more than 100 times the integrated luminosity of the data. Two-photon processes ($\gamma\gamma \rightarrow \ell^{+}\ell^{-}$ and $\gamma\gamma \rightarrow \mathrm{q\bar{q}}$) are also simulated with an integrated luminosity about three times that of the data.

For the signal, pair production of stable singly-charged particles is simulated for masses between 45 and 86 GeV/c^2. These particles are treated as heavy muons by the detector simulation program.

4   Low- and intermediate-mass selections

A preselection is applied to reject topologies which are clearly incompatible with pair-production of back-to-back, massive, long-lived particles. Exactly two tracks are required,

---

[1]The 172 GeV sample includes 1.1 pb^{-1} collected at 170 GeV.

both of which must be well reconstructed in the TPC. Both tracks must lie away from the beam axis ($|\cos\theta| < 0.90$), have at least one hit in the ITC, and satisfy the conditions $|d_{01}| + |d_{02}| < 0.3$ cm and $|z_{01}| + |z_{02}| < 5$ cm, where d_0 (z_0) is the distance of closest approach to the beam axis in the transverse plane (to the interaction point along the beam direction). The two tracks must have transverse momenta with respect to the beam axis, p_T, greater than $0.1\sqrt{s}$, equal momenta within three times the estimated error derived from the track fit, and the angle between them (acollinearity) must be greater than $160°$. Both tracks must fail the electron identification cut [10], and deposit less than 20 GeV (50 GeV) in the ECAL (HCAL). An event is rejected if it contains a photon with energy above 250 MeV or if energy deposits are detected in the luminosity calorimeters.

The acollinearity cut rejects radiative Z returns and two-photon processes. The cuts on p_T and the equal momentum requirement suppress two-photon and $\tau^+\tau^-$ backgrounds. The photon veto rejects radiative Z returns and Bhabha events. The cuts on electromagnetic and hadronic energy further improve Bhabha rejection, the latter being relevant when the electrons enter an ECAL insensitive region.

After this preselection, a large $\mu^+\mu^-$ background still survives, since the large mass of the signal has not yet been exploited. Two further sets of selection criteria, based on the measured particle masses $m_{1,2}$, defined as $m_i = \sqrt{E_{\text{beam}}^2 - p_i^2}$, are therefore introduced.

The so-called low-mass selection requires the two particles to have masses in the range $0.52 < m_{1,2}/E_{\text{beam}} < 0.80$ and an acollinearity greater than $174°$. In this mass range, the momenta of the tracks are high enough to produce an energy loss similar to that of ordinary particles; therefore dE/dx information is not used.

The intermediate-mass selection requires masses in the range $0.80 < m_{1,2}/E_{\text{beam}} < 0.98$ and a specific ionization $(R_{\mu 1} + R_{\mu 2}) \geq 10$. Here R_μ is an estimator calculated by comparing the measured dE/dx, I, to that expected for a muon $\langle I_\mu \rangle$: $R_\mu = (I - \langle I_\mu \rangle)/\sigma_I$, where σ_I is the expected resolution of the measurement. In order that a single track saturating the TPC electronics does not suffice for the event to be selected, this estimator is assigned a value of 5 when saturation prevents a direct dE/dx measurement.

For events with both masses in the range 90–98% of the beam energy the equal momentum requirement is relaxed, since the expected background (mainly $e^+e^- \rightarrow \tau^+\tau^-$) is lower in this mass region.

The only backgrounds surviving these cuts originate from the di-lepton channels, with cross sections of 10.4 fb for $\mu^+\mu^-$ and 1.2 fb for $\tau^+\tau^-$. This corresponds to an expected background of 0.3 events in the full data sample.

5   High-mass selection

The extension of the search to masses approaching the kinematic limit ($m/E_{\text{beam}} \simeq 1$) requires a somewhat different approach than the low- and intermediate-mass analyses. Particles with masses within a few percent of the kinematic limit ionise so heavily that the TPC digitising electronics saturate and neither high-resolution spatial coordinates nor reliable dE/dx measurements are available. Saturation occurs at approximately 25 times minimum-ionization. Saturated hits are not used by the standard ALEPH tracking since they have a resolution much worse than typical, unsaturated data. Nevertheless, the presence of many saturated channels is itself a distinctive feature of a high-mass signal

and in a clean two-track topology the characteristic pattern of a charged particle helix can be easily recognised from the spatial distribution of saturated hits.

The ITC amplifiers do not saturate, but the limited resolution in the z coordinate and the short lever-arm afforded by the ITC do not allow a kinematic selection based on tracks reconstructed with this detector alone. The high-mass selection requires exactly two tracks reconstructed in the ITC, which may or may not have (unsaturated) TPC hits associated to them. Events with energy deposited in the luminosity detectors are rejected. Energy deposits in the ECAL and HCAL are used to provide a three-dimensional point on each track candidate and verify a roughly back-to-back topology. The two most energetic calorimeter objects are selected; they must have an acollinearity of at least 160°, opposite polar angles within 8.5°, and each contain at least 50% of the calorimetric energy deposited on their side of the detector (defined by a plane containing the interaction point and perpendicular to the beam direction). Since low-β, massive particles should not shower in the calorimeters, the energy of these objects must be less than 5 GeV.

The positions of the two selected calorimeter objects, used as estimates of where the particles may have exited the tracking volume, and the position of the interaction point, used as an estimate of the origin of these particles, provide enough information for a single-helix fit of the transverse momentum and polar angle of the two track candidates. The reconstructed helix must cross at least four TPC pad rows on each side of the detector. The particle masses $m_{1,2}$ must be between 90 and 99.5% of the beam energy.

The estimated particle trajectories from the single-helix fit do not rely on any information from the tracking detectors, so the pattern of all hits (saturated and unsaturated) in the ITC and TPC can be checked for consistency. An approximatively 5 standard deviations road is defined around the single-helix trajectory; this road has a width of 1 cm (in $r\phi$) for the ITC, and 5 cm (in both $r\phi$ and z) for the TPC. At least 60% of the ITC layers and 40% of the TPC pad rows crossed by the road must contain a hit; this confirms the presence of charged tracks where predicted by the fit to calorimeter objects. The fairly low occupancy requirement in the TPC allows a track which projects onto a crack between outer sectors to be retained if every pad row in the inner sectors contains a hit.

Finally, the high mass of both particles is confirmed by the dE/dx measurements (if available) or by saturation of the TPC wires or pads (if not) by requiring either $R_{\mu 1} + R_{\mu 2} \geq 10$ or $f_{\text{sat}} > 0.33$; f_{sat} is the fraction of TPC pad rows crossed by the fitted helix which contain a saturated coordinate within the 5 cm road.

No background from the simulation survives the high-mass selection.

6   Efficiency

The final selection is a combination of the low- and intermediate-mass criteria (including their common preselection), and the complementary high-mass analysis. Together, the three selections yield an efficiency rising gently from 50% at $m/E_{\text{beam}} = 0.50$ to 70% at $m/E_{\text{beam}} = 0.90$; this is shown in Fig. 1 where the selection efficiency (including the trigger) for spin-1/2 stable charged particles is plotted as a function of m/E_{beam}.

For $m/E_{\text{beam}} > 0.993$ the particles stop in the calorimeters because of the high energy loss. In this case, if the particles are not stable and decay in the calorimeters, they

might produce additional energy deposits which will affect the selection efficiency. In the Goldstino scenario (long-lived sleptons) the energy release can be important and the efficiency is conservatively assumed to be zero. However in the high mass-degeneracy scenario (long-lived charginos) almost all the energy is taken by the neutralino and only a few hundred MeV are deposited in the calorimeters. In this case the efficiency is assumed to be equal to that of stable particles.

The efficiency depends on the spin (i.e., the production angular distribution) and mass of the charged particle. In the Monte Carlo signal generation, massive particles are produced with a flat angular distribution. The spin-1/2 and spin-0 efficiencies are derived from the generated signal by rescaling the angular acceptance using the formulae

$$
\begin{aligned}
\frac{d\sigma(\text{spin} = 0)}{d\Omega} &\propto \frac{\beta^3}{s} \sin^2\theta \\
\frac{d\sigma(\text{spin} = 1/2)}{d\Omega} &\propto \frac{\beta}{s} \left[1 + \cos^2\theta + (1 - \beta^2)\sin^2\theta \right] \ .
\end{aligned}
\tag{1}
$$

The expression for the differential spin-1/2 cross section is valid for s channel production under the assumption of purely vector coupling to spin-1 bosons.

To account for the dependence on $\sqrt{s}$, all cuts are performed in terms of variables normalised to the beam energy and the efficiency is parametrized as a function of m/E_{beam}. The trigger efficiency has been estimated with a Monte Carlo program simulating the two ALEPH triggers briefly described in Section 2. The trigger efficiency exceeds 99% for $m/E_{\text{beam}} \leq 0.97$, crosses 99% at $m/E_{\text{beam}} \simeq 0.98$, and finally decreases to 80% for $m/E_{\text{beam}} > 0.99$.

7 Systematic checks

For all variables used in the selections, good agreement exists between data and Monte Carlo simulation. The most important variables used to isolate the signal events are the measured momenta and dE/dx of the two particles. The uncertainty on the beam energy has a negligible impact on the results. The tracking performance was tested with data at the Z peak with a variety of techniques (see for example [11]), showing agreement of the absolute momentum calibration between data and Monte Carlo better than ~ 100 MeV/c for 45 GeV/c tracks. This level of momentum uncertainty has a negligible impact on the analysis.

Studies of dE/dx performance at the Z peak have been described in many ALEPH papers (see for example [12]). Additional studies were performed with the 1996 data, using minimum-ionising pions, identified muons, and electrons identified using the ECAL information. Agreement of the absolute dE/dx calibration is obtained between data and Monte Carlo at the level of ~ 0.3 times the expected resolution, which is $\sim 4.5\%$ for high energy isolated electrons. The 1996 data exhibit a dE/dx resolution 10–20% better than the Monte Carlo which goes in the direction of increasing the selection efficiency. These effects lead to a very small change ($< 1\%$) of the selection efficiency since the dE/dx information is only used in a β region when the expected ionization is much larger than the cut applied in the analysis.

For the high-mass selection, the identification of pair-produced charged tracks using calorimeter objects has been tested using di-muon events collected at the Z peak. Although muons produced in Z decays do not ionise heavily enough to saturate the TPC electronics, the high-mass signal can be simulated with data by applying to di-muon hits the same algorithm used for saturated coordinates. The resulting TPC hit positions agree with those of the standard ALEPH reconstruction to within about half the width of a cluster on the pad row in $r\phi$ (~ 1 cm) or half the pulse-length in z ($\ll 1$ cm).

The transverse spatial resolution of the ECAL entry point used in the fit is roughly 1.5 cm, consistent with the granularity of the ECAL towers. The longitudinal uncertainty on the entry point is expected to be of the order of one radiation length in lead, or less than 2 cm, and in any case has only a second-order effect on the fit.

A conservative 5% systematic error on the selection efficiency has been applied. The impact of this systematic error on the cross section upper limit has been calculated according to the method described in Ref. [13], based on the convolution of the Poisson probability estimator with a Gaussian of sigma equal to the error on the signal efficiency.

8 Results

No event in the 172 GeV data survives any of the three selections. This sets the 95% confidence level upper limits on the production cross section which are plotted as dashed curves in Fig. 2 and 3 for spin-1/2 and spin-0 particles, respectively. No candidate is found in the data samples collected at $\sqrt{s} = 161$, 136 and 130 GeV, allowing the cross section limit to be improved.

The corresponding integrated luminosities must be rescaled to account for the dependence on $\sqrt{s}$ of the spin-0 and spin-1/2 production cross sections shown in Eq. 1. The combined upper limit at 95% CL is

$$\sigma_{172} \leq \frac{3}{(\mathcal{L}_{172}\epsilon_{172} + \mathcal{L}_{161}^{\mathrm{res}}\epsilon_{161} + \mathcal{L}_{136}^{\mathrm{res}}\epsilon_{136} + \mathcal{L}_{130}^{\mathrm{res}}\epsilon_{130})} \ ,$$

where $\mathcal{L}^{\mathrm{res}}$ denotes the rescaled luminosities and ϵ the selection efficiencies. The improved limits obtained by including the data at lower energies are shown as thick curves in Fig. 2 and 3. Cross sections of 0.2–0.4 pb at $\sqrt{s} = 172$ GeV are excluded at 95% CL for masses between 45 and 86 GeV/c^2, almost independently of the mass and spin of the heavy particle.

As already mentioned, the possibility of a long-lived charged scalar lepton depends, in the model of Ref. [3], on the value of the SUSY breaking scale parameter $\sqrt{F}$; the requirement that the particle decay outside the detector therefore constrains this scale. In Fig. 4 the cross section limit is plotted as a function of m and $\sqrt{F}$. The lifetime-dependence of the efficiency is approximated with a factor $\exp\left(-2\ell_{\mathrm{det}}/\beta\gamma c\tau\right)$, where $\ell_{\mathrm{det}} = 8.5$ m is the maximum length travelled by a particle inside the detector. The limit on the cross section worsens for scales below 500–1000 TeV.

These cross section upper limits can be translated into lower limits on the masses of charginos and sleptons with long lifetimes. The cross sections expected in the MSSM [14] for charginos and for right- and left-handed smuons or staus are also shown in Fig. 2 and 3, respectively. The selectron production cross section also depends on the neutralino masses

and couplings due to neutralino exchange in the t channel, therefore no general mass limits can be given. For charginos the cross section range displayed in Fig. 2 was determined as follows: a value of $\tan\beta = \sqrt{2}$ was chosen; a given chargino mass then defines a relation between M and μ (where μ is the supersymmetric mass term which mixes the two Higgs superfield); for each pair of M and μ values, the gauge unification condition was relaxed and M' varied up to 5 M; if the condition $m_{\tilde{\chi}^\pm} - m_{\tilde{\chi}^0} \leq 200$ MeV/c^2 could be satisfied in that way, the chargino production cross section was calculated, assuming a sneutrino mass of 250 GeV/c^2.

The lower 95% confidence level mass limits for long-lived smuons or staus are 67 and 69 GeV/c^2 for right- and left-handed particles, respectively. For a long-lived chargino, due to the large production cross section, the kinematic limit of 86 GeV/c^2 is almost attained.

9   Conclusions

ALEPH data collected at 172, 161, 136 and 130 GeV yield a 95% confidence level upper limit of 0.2–0.4 pb on the pair-production cross section at 172 GeV of long-lived, singly-charged particles with masses between 45 and 86 GeV/c^2. This cross section limit implies, in the MSSM, lower limits of 67 GeV/c^2 on the mass of right-handed staus and smuons and of 69 GeV/c^2 on the mass of left-handed staus and smuons. For long-lived charginos a lower mass limit of $\sim$ 86 GeV/c^2 has been obtained.

Acknowledgements

References

[1] H. Nilles, Phys. Rep. **C 110** (1984) 1;
    H. Haber and G. Kane, Phys. Rep. **C 117** (1985) 75;
    R. Barbieri, Riv. Nuovo Cimento **11**, (1988) 1.

[2] G. Altarelli et al., *Physics at LEP 2*, CERN 96-01.

[3] S. Dimopoulos et al., Nucl. Phys. Proc. Suppl. **52A** (1997) 38; Phys. Rev. Lett. **76** (1996) 3494.

[4] H. Dreiner and G.G. Ross, Nucl. Phys. **B 410** (1993) 188.

[5] The DELPHI Collaboration, Phys. Lett. **B 247** (1990) 157.

[6] The OPAL Collaboration, Phys. Lett. **B 252** (1990) 290.

[7] The ALEPH Collaboration, Phys. Lett. **B 303** (1993) 198.

[8] The DELPHI Collaboration, *Search for Stable Heavy Charged Particles in e^+e^- Collisions at $\sqrt{s}$= 130-136, 161 and 172 GeV*, CERN-PPE/96-188.

[9] The ALEPH Collaboration, Nucl. Instr. and Meth. **A 294** (1990) 121.

[10] The ALEPH Collaboration, Nucl. Instr. and Meth. **A 360** (1995) 481.

[11] The ALEPH Collaboration, Phys. Lett. **B 349** (1995) 585.

[12] The ALEPH Collaboration, Phys. Lett. **B 388** (1996) 648.

[13] R.D. Cousins and V.L. Highland, Nucl. Instr. and Meth. **A 320** (1992) 331.

[14] Code written by G.R. Ridolfi based on:
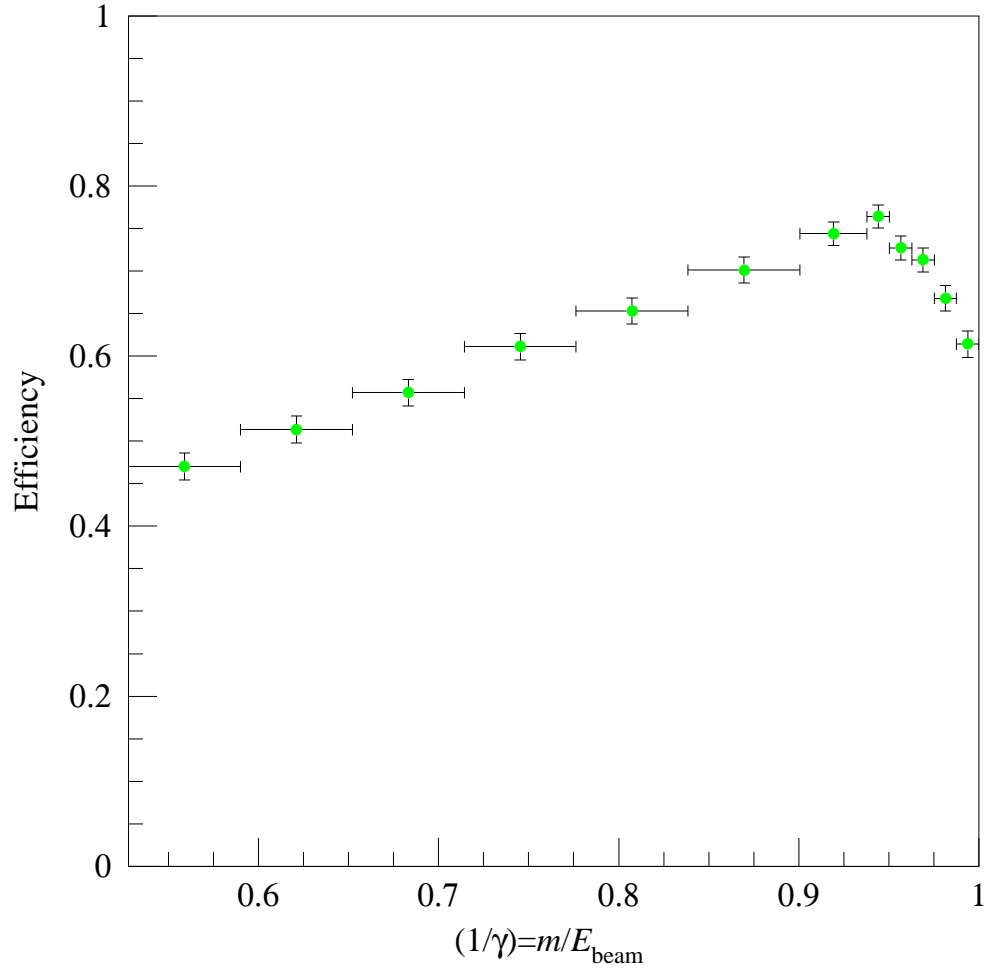   A. Bartl, H. Fraas and W. Majerotto, Z. Phys. **C 30** (1986) 441; **C 34** (1987) 411.

Figure 1: Selection efficiency as a function of m/E_{beam} for spin-1/2 stable charged particles. The efficiency curve for spin-0 particles has a similar shape but is slightly higher, owing to the larger fraction of cross section within the geometrical acceptance of the selection.
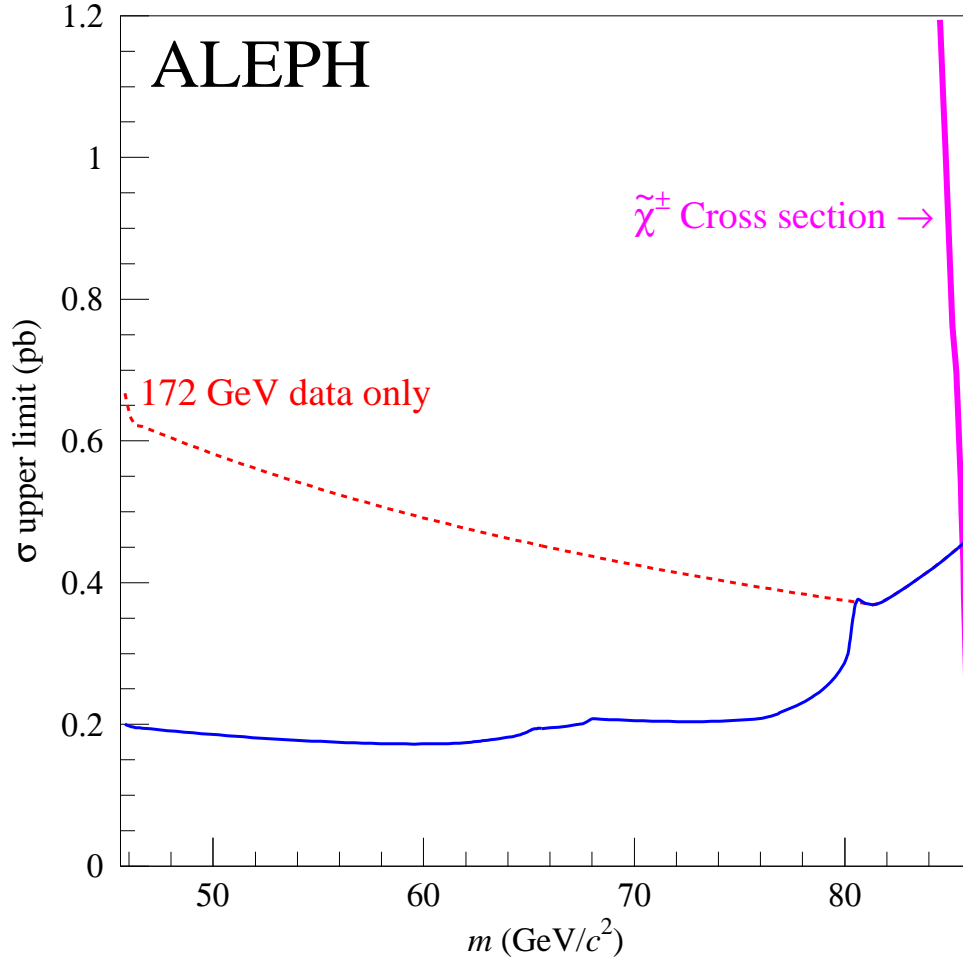
Figure 2: 95% CL upper limit on the production cross section for spin-1/2 particles at $\sqrt{s} = 172$ GeV, as a function of mass. The dashed curve shows the limit obtained from the 172 GeV data set alone, while the thick solid curve shows the limit obtained by adding the 161, 136 and 130 GeV data to the analysis. The band on the right shows the chargino cross section calculated as described in Section 8.
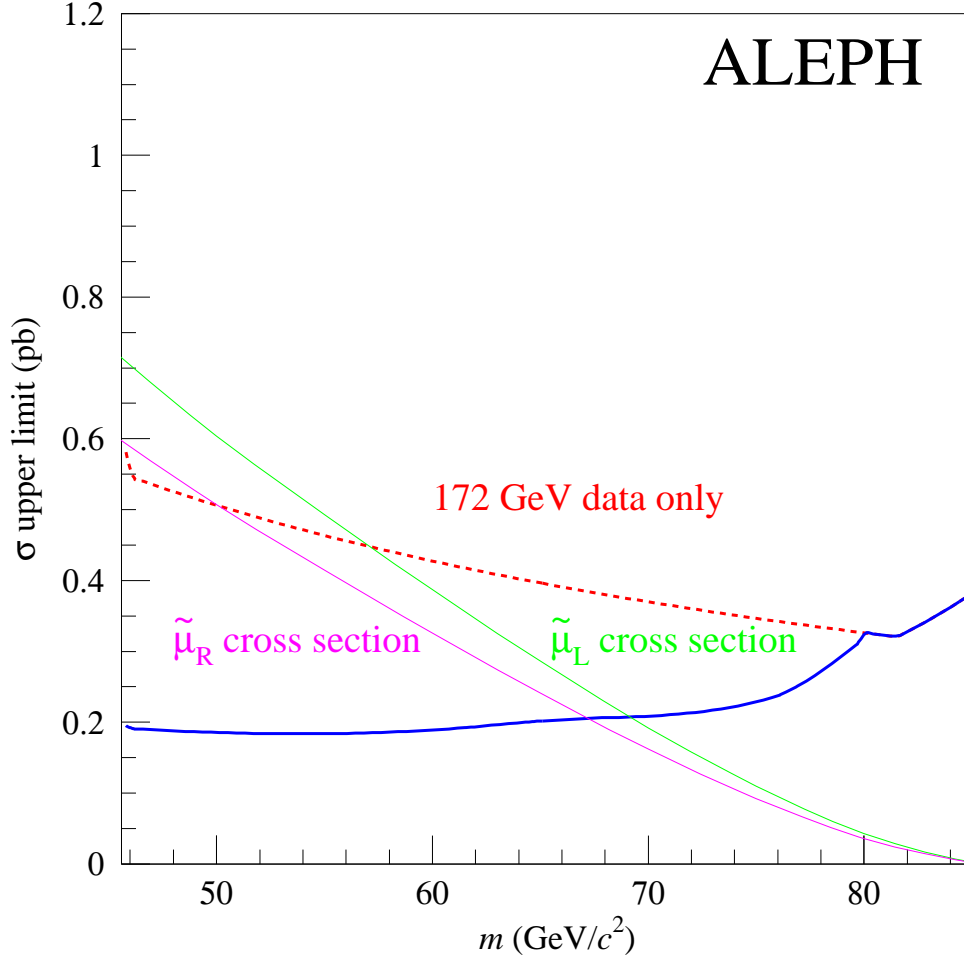
Figure 3: 95% CL upper limit on the production cross section for spin-0 particles at $\sqrt{s} = 172$ GeV, as a function of mass. The dashed curve shows the limit obtained from the 172 GeV data set alone, while the thick solid curve shows the limit obtained by adding the 161, 136 and 130 GeV data to the analysis. The left-handed and right-handed scalar-muon (or scalar-tau) production cross sections are superimposed.
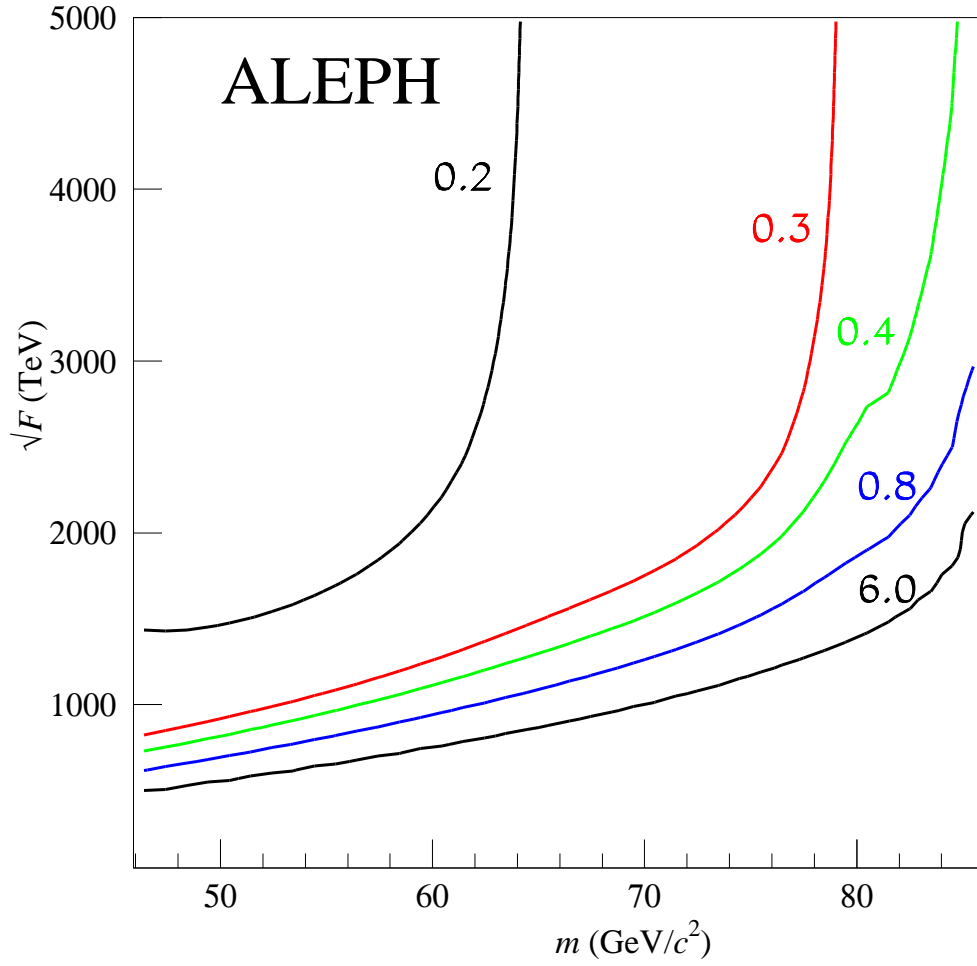
Figure 4: 95% CL upper limits (in pb) on the production cross section for spin-0 particles at $\sqrt{s} = 172$ GeV as a function of mass and SUSY-breaking scale, $\sqrt{F}$.